2008 American Control Conference
Westin Seattle Hotel, Seattle, Washington, USA
June 11-13, 2008

Combined H_∞-Feedback and Iterative Learning Control Design with Application to Nanopositioning Systems

B.E. Helfrich, C. Lee, D.A. Bristow, X.H. Xiao, J. Dong, A.G. Alleyne, *Senior Member, IEEE*, S.M. Salapaka, *Member, IEEE*, and P.M. Ferreira

***Abstract*—This paper presents a coordinated design framework for precision motion control (PMC) systems. In particular, the focus is on the design of feedback and feedforward controllers operating on systems that repeatedly perform the same tasks. The repetitive nature of the tasks suggests the use of Iterative Learning Control (ILC). However, in addition to the repeatability of the desired trajectory, the class of systems under study examines the effect of non-repeating disturbances and possible reset errors. The rejection of uncertain, but bounded, disturbances suggests the use of H_∞ design. The non-repeating disturbances and reset errors necessitate coordination of the feedback and feedforward designs. The assumption that the disturbances have a particular frequency distribution affords a frequency domain separation between the two controller degrees of freedom. Experimental results are given on a piezo-driven nano-positioning device demonstrating the benefits to the presented approach.**

I. Introduction

Precision motion control (PMC) [1],[2] is an important research area with high relevance to advanced technology including high precision imaging and manufacturing. High precision systems can utilize feedback or feedforward control designs or a combination of both feedforward and feedback in a two-degree-of-freedom approach. Effective feedback design tools include H_∞ feedback control [3],[4]. Additionally, for systems that repeat the same trajectory, as in the case of manufacturing, Iterative Learning Control (ILC) [5]-[8] is a good choice for feedforward control design. The goal of this article is to present a frequency-based design methodology to improve the overall system performance by delegating the roles of feedback and ILC controllers based on known classes of exogenous signals.

This investigation is motivated by physical phenomena. The class of physical systems under consideration consists of a structure, possibly multi-degree-of-freedom, which is driven by some type of actuation device. These could be small flexure-based structures with piezo actuators, as with Atomic Force Microscope stages [9], or large inertias driven electromagnetically, such as silicon wafer scanning stages [10]. By design, these systems tend to have well defined dynamics in the low frequency range, where "low" is relative to the 1st structural resonance. For the flexure-based systems, the dynamics are essentially a gain; for the inertia systems, the dynamics are essentially a double integrator. Above the first structural resonance, there are usually higher order structural modes that are lightly damped and position dependent thereby making them difficult to compensate with control. A clear identification of the known dynamics in the frequency domain suggests the use of modern robust control design tools such as H_∞ feedback controllers [11]. These tools are good for point to point regulation and lower frequency tracking.

For higher frequency tracking, it is advantageous to include a feedforward controller in the PMC system. The feedforward controller is usually an approximate inverse of the plant. For trajectories that repeat themselves, a very successful approach is to instead learn the feedforward signals for subsequent trials by iteratively updating them based on the error accumulated in previous trials. This approach has been formalized as ILC [5]-[8]. ILC has the benefit of not requiring a plant model yet still giving high performance tracking inputs. While an explicit plant model is not required, it can often be useful in the design of the ILC to minimize the number of iterations taken to converge to an appropriate feedforward input signal.

The primary assumptions for ILC systems include the fact that all exogenous signals, i.e. references and disturbances, are identical from trial to trial. Additionally, current ILC practice assumes that the initial conditions for the system are also identical at the start of each trial. As will be seen, those assumptions are violated in the current work necessitating a modification to current ILC practice. In particular, this work examines the effect of non-repeating disturbances and imperfect resetting on ILC systems. Additional investigations focus on how a good design procedure, combining feedback and ILC, can mitigate these effects.

The rest of the paper is organized as follows. Section 2 gives a brief background for the design of both H_∞ and ILC control schemes. This gives a common platform to describe coordination. Section 3 presents the overall design strategy employed to coordinate the two controller degrees of

This work was supported in part by the University of Illinois at Urbana-Champaign Nano-CEMMS center NSF Award #0328162.

A.G. Alleyne, J. Dong, P.M. Ferreira, B.E. Helfrich, C. Lee, S.M. Salapaka and X.H. Xiao are with the Mechanical Science and Engineering Department at the University of Illinois at Urbana-Champaign, Urbana, IL 61801 USA (phone: 217-244-9993; fax: 217-244-6534; e-mail: respectively, alleyne@uiuc.edu, pferreir@uiuc.edu, bhelfri2@uiuc.edu, clee62@uiuc.edu, salapaka@uiuc.edu, xhxiao@uiuc.edu).

D.A. Bristow is with the Department of Mechanical and Aerospace Engineering, Missouri University of Science and Technology, Rolla, MO.

freedom. Key to the coordination is the knowledge of relative signal power between repeatable and non-repeatable signals in the frequency spectrum. Section 4 presents a simulation example demonstrating the coordination. A key part of the simulation example is the demonstration of non-repeating initial conditions that can occur when utilizing piezo actuation systems that have hysteresis as part of their dynamics. The simulation example is based off the experimental system used to present the results in Section 5. The experimental results support the simulation findings as well as the design procedure of Section 4. A conclusion then summarizes the main points of the paper.

II. Controller Background

The PMC system architecture is depicted in Figure 1. Components of the system include the feedback controller, *K(z)*, iterative learning controller, ILC, and the plant model, *G(z)*. Signals identified in the diagram are the reference, *r*(z), error, e_j(z), feedback control, v_j(z), learning control, u_j(z), repeatable output disturbance, *d*(z), nonrepeatable output disturbance, d_j(z), noise n_j(z), and the output signal, y_j(z). The variable '*z*' indicates that the analysis is performed in discrete time; whereas, the subscript '*j*' denotes each signal's iteration.

In the design and analysis throughout this paper, the following assumptions were made to simplify calculations.

- All signals are assumed to be over an infinite time horizon for frequency domain design.
- The noise n_j(z) and non-repeating disturbance d_j(z) is assumed to have an expected value, or mean, of zero.

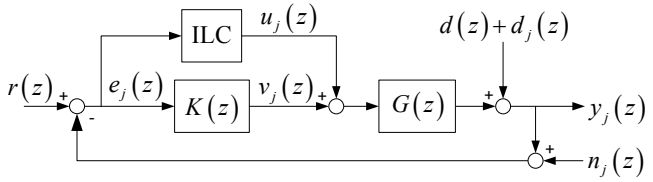

Figure 1 - Block Diagram of Feedback and ILC System

2A. Stand-alone H_∞ Feedback Control Design

In a stand-alone feedback controller design, the main objective is to achieve performance (*i.e.* bandwidth) and high resolution (*i.e.* disturbance and noise attenuation) with uncertainties in the operating environment. Both components are vital in achieving precision motion control. The classical control design processes such as PID require an exhaustive search over the space of controller parameters to meet bandwidth and resolution requirements. The advantage of H_∞ robust control is that the objectives of performance, resolution, and robustness to model uncertainty can be directly considered in the frequency domain via appropriate weighting functions. Then a mathematical optimization framework can be utilized to numerically search for a design.

In H_∞ design, the closed-loop transfer functions *S(z)*, *T(z)*, and *KS(z)* have the definitions

$$S(z)=\frac{y_j(z)}{d_j(z)}=\frac{y_j(z)}{d(z)}=\frac{1}{1+G(z)K(z)}, \tag{1}$$

$$T(z)=\frac{y_j(z)}{r(z)}=\frac{G(z)K(z)}{1+G(z)K(z)}, \tag{2}$$

$$KS(z)=\frac{v_j(z)}{r(z)}. \tag{3}$$

In the stand-alone feedback design, we assume $u_j(z)=0$, and thus, the error signal is given by,

$$\begin{aligned} e_j(z) &= r(z)-y_j(z) \\ &= S(z)r(z)-S(z)d(z)-S(z)d_j(z)+T(z)n_j(z). \end{aligned} \tag{4}$$

Eqn. 4 indicates that in order to decrease the tracking error, both *S(z)* and *T(z)* should be small. The sensitivity function, *S(z)*, needs to be small in order to mitigate the effects of $\{r(z),d(z),d_j(z)\}$ on the error. The complementary sensitivity function, *T(z)*, needs to be small to mitigate the effects of noise, $n_j(z)$ on the error. Satisfying both *S(z)* and *T(z)* small is not possible due to the algebraic limitation

$$S(z)+T(z)=1. \tag{5}$$

The H_∞ control signal is given by,

$$\begin{aligned} v_j(z) = KS(z)r(z)-KT(z)\big(d(z)+d_j(z)\big) \\ -KS(z)n_j(z) \end{aligned}. \tag{6}$$

Note, when saturation of the control output becomes a concern [13], we will require a bound on *KS(z)*.

While designing the controller, the performance objective of a small tracking error, high bandwidth, and robustness to uncertainty cannot be satisfied simultaneously. This inevitable tradeoff can be explained by the Bode Integral law [12]-[14]. The Bode Integral is given in (7).

$$\int_{-\pi}^{\pi}\log\left|S(z)\right|dz=0 \tag{7}$$

Thus if $|S(z)|$ needs to be small at low frequency for small tracking error, this will create large magnitude in *S(z)* at a different frequency region. The result of increasing *S(z)* is a decrease in the system's closed loop bandwidth, where the bandwidth is defined at the crossover frequency or $|S(z)|=-3dB$ [4]. This phenomenon is known as the "waterbed" effect [4], and it serves to illustrate that there is always a fundamental tradeoff and limitation among bandwidth, robustness, and tracking error.

The controller transfer function, *K(z)*, is obtained through an iterative design of weighting functions to minimize

$$\gamma=\left\|\begin{matrix} W_S(z)S(z) \\ W_T(z)T(z) \\ W_V(z)KS(z)\end{matrix}\right\|_\infty, \tag{8}$$

where $\|X(z)\|_\infty=\max_{\omega\in[-\pi,\pi]}\left|X\left(e^{i\omega}\right)\right|$. The weighting functions $\{W_S(z),W_T(z),W_V(z)\}$ achieve the design objective by shaping the controller. Solutions to this problem are well known [15], and iterative numerical techniques are widely

available, for example in MATLAB software [16]. In the following, we summarize standard guidelines for the solution of $W_S(z)$, $W_T(z)$, and $W_V(z)$. The interested reader is referred to [3],[4] for a more detailed discussion.

The transfer function, $W_S(z)$, is typically chosen to have high gains at low frequencies and low gains at high frequencies. This scaling ensures that the optimal feedback law is such that the sensitivity function is small at low frequencies, thereby guaranteeing good tracking at the frequencies of interest. The weighting function, $W_T(z)$, is often chosen such that it has high gains at high frequencies and low gains at low frequencies. This is done in attempt to shape $T(z)$ such that it rolls off at high frequencies for noise attenuation. The weighting function for the control, $W_V(z)$, is chosen to ensure that the control signals remain within saturation limits to prevent instability.

2B. Iterative Learning Control Design

Iterative learning control (ILC) [5]-[8] is used to improve the performance of systems that repeat the same operation many times. ILC uses the tracking errors from previous iterations of the repeated motion to generate a feedforward control signal for subsequent iterations. Convergence of the learning process results in a feedforward control signal that is customized for the repeated motion, yielding very low tracking error. For the purposes of the ILC design, we assume that the feedback controller is given, and therefore $S(z)$ is fixed. We find that the j^{th} iteration of the system in Figure 1 can be written as,

$$\begin{aligned} e_j(z) = -G(z)S(z)u_j(z) + S(z)\big(r(z) - d(z)\big) \\ - S(z)d_j(z) + T(z)n_j(z). \end{aligned} \tag{9}$$

As we will see, a fundamental limitation of ILC is the inability to compensate for the non-repeating disturbances, $d_j(z)$.

In this work we consider first-order ILC algorithms of the form,

$$u_{j+1}(z) = Q(z)\big(u_j(z) + L(z)e_j(z)\big). \tag{10}$$

The learning function, $L(z)$, maps the error signal to the control signal, and the filter $Q(z)$ is used to limit the frequency range of the learning for stability and noise attenuation. The well-known ILC stability condition [6] is

$$\left\| Q(z)\big(1 - L(z)P(z)\big) \right\|_\infty < 1. \tag{11}$$

For fast convergence [8], we select $L(z)=S^{-1}(z)G^{-1}(z)$. Note that when $S(z)G(z)$ is strictly proper, $L(z)$ is improper. An improper learning function can be implemented by appropriately shifting the error signal during the learning process [8]. When $S(z)G(z)$ is non-minimum phase, then $L(z)$ is unstable, which can lead to large control signals. In this case the learning function can be separated into causal components and anticausal components and then stably filtered in the forward time with the causal component and then in negative time with the anticausal component [17].

Typically, there will be frequencies for which the system model is inaccurate. Eqn. (11) illustrates that for large uncertainties in some frequency range (e.g. gain uncertainty larger than 100%) we must have $|Q(z)| \ll 1$ in that frequency range for robust stability of the ILC.

The performance of the ILC at convergence is measured by the power spectrum of $e_\infty(z) \triangleq \lim_{j\to\infty} e_j(z)$. In the following the 'z' transfer function argument is dropped for compactness. We multiply (10) by GS,

$$GSu_{j+1} = QGSu_j + QGSLe_j. \tag{12}$$

Next, substituting (9) for GSu_j resulting in

$$\begin{aligned} -e_{j+1} + Sr + Sd + Sd_j + 1 - Sn_{j+1} = -Qe_{j+1} + QSr \\ + QSd + QSd_j - QSn_j + QLGSe_j \end{aligned}, \tag{13}$$

$$\begin{aligned} e_{j+1} = Q(1 - LGS)e_j + (Q-1)S(r-d) \\ - S\big(d_{j+1} + Qd_j\big) + S\big(n_{j+1} - Qn_j\big). \end{aligned} \tag{14}$$

Since $L=S^{-1}G^{-1}$, the e_{j+1} term conditionally depends on Q as,

$$e_{j+1} = \begin{cases} -S\big(d_{j+1} + d_j\big) + S\big(n_{j+1} - n_j\big) & \text{for } Q = 1 \\ -S(r-d) - Sd_{j+1} + Sn_{j+1} & \text{for } Q = 0 \end{cases}. \tag{15}$$

For those interested, further analysis is performed in [18].

The typical Q-filter design is a low pass filter [19]. This is because the system is usually well known at low frequencies, and non-repeating disturbances are minimized by the feedback controller at low frequencies. A tradeoff exists between minimizing repeatable error and amplifying noise when designing the Q-filter. When $Q=1$, the repeatable error is eliminated, but the noise is amplified. Alternatively, $Q=0$ has no effect on the noise or repeatable signal. Therefore, we want to vary the value of Q with respect to frequency. We should set $Q=1$ in frequency regions where the repeatable component, $S(r-d)$, is dominant, and set $Q=0$ where the nonrepeatable component, $S(d_j+n_j)$ is dominant.

III. Frequency-Delegated H_∞ and ILC Design

The previous two subsections, 2.A and 2.B, described independent design strategies for the feedback and ILC controllers. That is, the feedback controller was designed with complete disregard to the ILC, and the ILC was designed for a given stabilizing feedback controller. This section develops a frequency-delegation design strategy to coordinate the design of both controllers by delegating specific frequency bands for feedback and ILC operation. The following outlines the design heuristic.

The first task is to develop an accurate model of the system. This can be done by first principles or by system identification techniques. Next, the exogenous signals affecting the system must be identified by frequency range and as repeatable or nonrepeatable. For simplicity, we assume that noise only affects the system at high frequencies, and therefore our focus here is on the repeatable signals, $r(z)$ and $d(z)$, and the nonrepeatable $d_j(z)$.

Here we define the Repeatable-to-Nonrepeatable Ratio (RNR) of signal power as

$$\mathrm{RNR}(\omega) \equiv 20*\log\left(\frac{\left|FFT\left[r(z)-d(z)\right]\right|^2}{\frac{1}{N}\sum_{j=1}^{N}\left|FFT\left[d_j(z)\right]\right|^2}\right), \quad (16)$$

where N is the total number of iterations of the signal identification. The RNR is a useful metric for determining a frequency domain delegation of the control effort.

The RNR cannot be obtained directly because we cannot directly measure $d(z)$ and $d_j(z)$. In our approach we indirectly obtain the RNR from N iterations of the error signal history,

$$e_j(z) = S(z)\left(r(z)-d(z)\right) - S(z)d_j(z) + T(z)n_j(z), \quad (17)$$

$j = 1,\ldots,N$. Although this approach requires a feedback controller, we will show that our approach is insensitive to $S(z)$, and thus any stabilizing feedback will suffice. Using the error histories, we find the repeatable error as,

$$\bar{e}(z) = \sum_{j=1}^{N} e_j(z) \cong S(z)\left(r(z)-d(z)\right), \quad (18)$$

for large N. Then, for frequencies where noise n_j is small,

$$\begin{aligned} &20*\log\left(\frac{\left|FFT\left[\bar{e}(z)\right]\right|^2}{\frac{1}{N}\sum_{j=1}^{N}\left|FFT\left[\bar{e}(z)-e_j(z)\right]\right|^2}\right) \\ &= 20*\log\left(\frac{\left|FFT\left[S(z)\left(r(z)-d(z)\right)\right]\right|^2}{\frac{1}{N}\sum_{j=1}^{N}\left|FFT\left[S(z)d_j(z)\right]\right|^2}\right) \quad (19) \\ &= \mathrm{RNR}(\omega). \end{aligned}$$

Since both repeatable and nonrepeatable signals are scaled by $S(z)$, the ratio is insensitive to $S(z)$, and thus the feedback controller does not affect our estimate of the RNR.

Repeatable and nonrepeatable signals will have different amplitudes at different frequencies, as schematically depicted in Figure 2a, for the class of systems considered here. In 2a, the low frequency region is dominated by the nonrepeatable signal, which has significantly more energy than the repeatable signal. At higher frequencies the role is reversed. At the highest frequencies, both repeatable and nonrepeatable signals are sufficiently low in energy to be ignored.

The H_∞ feedback and ILC frequency delegation is illustrated by Figure 2a and 2b. In frequency regions where nonrepeating signals dominate, the H_∞ feedback controller should have maximum authority. Weighting functions, $W_S(z)$ and $W_T(z)$, for the H_∞ controller should be shaped as shown in Figure 2c and described in Table 1. As in the stand-alone feedback design in Section 2A, $W_V(z)$ should have high gain in the frequency regions where saturation of the control signal needs to be prevented.

Delegation of control authority is given to ILC in frequency ranges where the RNR is high. The Q-filter magnitude should be 1 in these regions and it should be 0 in the regions delegated to the feedback controller, where the RNR is low. Just as in Section 2B, the only caveat to the Q-filter design is that it should also be 0 in frequency regions where model uncertainty is large to achieve convergence, as in (11). The Q-filter design is illustrated in Figure 2d and Table 2.

Upon completion of the controller designs, experimental testing is required to evaluate performance results. A graphical layout of the procedure is shown in Figure 3. An iterative approach to the design process is suggested.

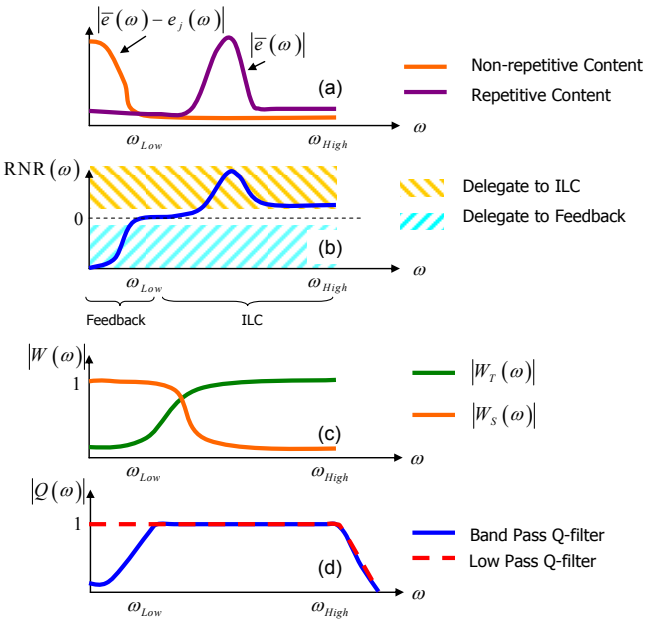

Figure 2 - Frequency Delegated Controller Design

Table 1 - H_∞ Design Summary as Function of Frequency

RNR	$\lvert W_S \rvert$	$\lvert W_T \rvert$
Small	Low	High
Large	High	Low

Table 2 - ILC Design Summary

Model Uncertainty	RNR	Q-filter
Large	N/A	$Q(\omega) = 0$
Small	Small	$Q(\omega) = 1$
Small	Large	$Q(\omega) = 0$

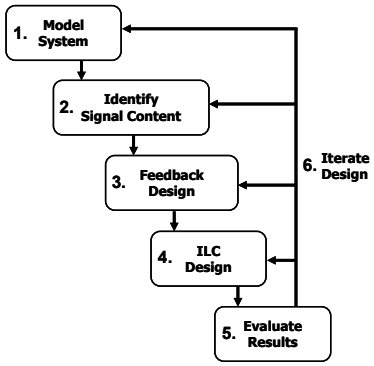

Figure 3 - Design Methodology Flowchart

IV. Simulation Example: Nanopositioner

The particular system example used here is a piezo-actuated flexure-based positioner. The positioning system used for the experimental results in Section 5 is a Physik Instrumente P-611.3S NanoCube XYZ Piezo Nano-positioning System and E-664 NanoCube Piezo Controller. The total range of motion for this device was 100 microns in the x, y and z directions, though here we consider motion only in the x-axis for the purpose of illustration. The frequency response of the system is shown in Figure 4. In order to include the high frequency resonances, the model's order becomes large, which possibly leads to greater sensitivity to model uncertainty. Model variations become apparent in the frequency response curves, as seen in Figure 4, and this creates more uncertainty about the estimated model of the system. For example, the phase plot shows that the 50 mV and 100 mV curves are completely out of phase around 170 Hz from system ID tests. This model uncertainty could lead to ILC instability and can be mitigated by "rolling off" the Q-filter.

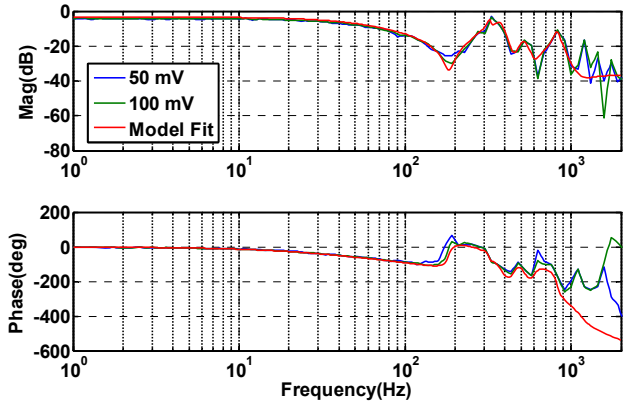

Figure 4 - System ID Frequency Response Plot

System ID tests estimate a 12th order discrete LTI model, (20), which consisted of several high frequency resonances as shown in Figure 4. Above 100 Hz, the model has several complex pole-zero pairs, which create difficulties for tracking reference signals above this frequency. Controller designs and reference signals did not attempt to operate in the frequency band greater than 100 Hz.

$$G(z)=\frac{\begin{array}{l}0.025031(z-0.5323)(z^2-1.891z+0.9723)\\(z^2-1.703z+0.9595)(z^2-1.462z+0.9289)\\(z^2-1.109z+0.8855)(z^2-0.4932z+1.719)\end{array}}{\begin{array}{l}(z-0.6193)(z-0.9251)(z^2-1.294z+0.5162)\\(z^2-1.723z+0.9719)(z^2-1.589z+0.9055)\\(z^2-1.268z+0.8754)(z^2-0.502z+0.8917)\end{array}} \quad (20)$$

Piezo actuators, such as those that drive this device, suffer from a hysteretic behavior. Hysteresis is a nonlinear phenomenon [20], that can be difficult to precisely control. Figure 5 shows data from the experimental system that was used to augment the linear model in (20). Hysteresis models [20] often include an internal state variable to capture the direction dependent characteristics. When the positioner is reset to an initial condition to start a trajectory, the internal hysteresis state is nonzero. This means that a nonzero initial input signal is required to initiate movement of the piezo. The net effect of this is a path dependent reset. Even though the positioner is at the same initial position at the start of a repetitive trajectory, the internal hysteretic state can vary depending on the exact path taken to reset the positioner. This nonlinear hysteresis results in an example of a low frequency non-repeating exogenous signal to the positioning loop. Figure 6(top) shows the periodogram of the x-position output from the nanopositioning system shown in Section 5. The hysteresis is the low frequency nonrepeatable content.

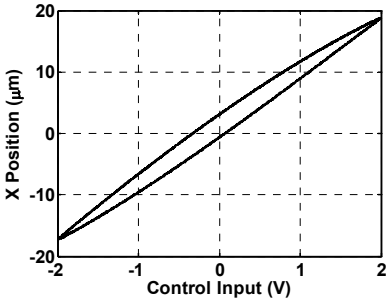

Figure 5. Hysteresis Plot w/ Open Loop Inputs

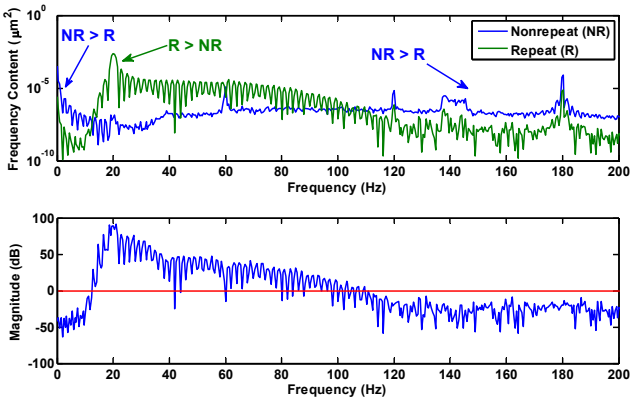

Figure 6. (top) Repeatable, *d(z)*, and Nonrepeatable, $d_j(z)$, Signal Periodogram (bottom) RNR of Signal Power

Simulation and experimental results use a modified 20Hz sinusoidal signal with 3 micron magnitude for *r(z)*. The modification is band pass filtering *r(z)*, such that repetitive signal content is large in the region around 20Hz and small at other frequencies. From the experimental system in Section 5, the low frequency effects of hysteresis are combined with the 20Hz reference signal into the RNR as shown in Figure 6(bottom), the total exogenous signal set resembles the case shown in Figure 2c. We see a clear frequency separation of the exogenous repetitive and nonrepetitive signals. The frequency region between 10-30Hz (mid-range frequency) contains the repetitive content, whereas the large stochastic signals occur below 10Hz and above 100 Hz.

Overall, four basic control schemes are considered to

explore the scenario given in Figure 2. Two feedback controllers were designed with different closed loop bandwidths. One controller was designed to mitigate the effects of all low frequency error, and this system's closed loop bandwidth was approximately 15 Hz. Indeed, this system does reduce low frequency error, but when tracking the 20 Hz reference signal, the error signal is large. The second feedback controller's design intention was to be a stand-alone controller. With a bandwidth of 44 Hz, this second controller had low tracking error for the 20 Hz sine wave reference. Since these two controllers have distinctly different bandwidths, they will be referred to as the low bandwidth (K_{LBW}) and high bandwidth (K_{HBW}) controller, (21) and (22), respectively. The bode plots can be viewed in Figure 7. Note that, due to (7), there is a tradeoff between the controller's bandwidth and its low frequency gain. The H_∞ design allows the low bandwidth controller to have a larger DC gain by constraining the bandwidth.

$$K_{LBW}(z)=\frac{\begin{array}{l}0.12369(z+1)(z+0.5941)(z-0.6718)^2\\(z-0.6135)(z-0.925)(z^2-1.974z+0.9744)\\(z^2-1.309z+0.5305)(z^2-1.734z+0.9736)\\(z^2-1.611z+0.9125)(z^2-1.338z+0.8926)\\(z^2-0.7768z+0.9227)\end{array}}{\begin{array}{l}(z+0.9436)(z-0.8987)(z-0.9969)^3(z-0.5293)\\(z^2-0.8514z+0.2412)(z^2-1.788z+0.8715)\\(z^2-1.716z+0.9621)(z^2-1.479z+0.8829)\\(z^2-1.27z+0.8531)(z^2-0.7288z+0.8641)\\(z^2-1.611z+0.9125)(z^2-1.338z+0.8926)\end{array}} \quad (21)$$

$$K_{HBW}(z)=\frac{\begin{array}{l}0.56966(z+1)(z+0.8803)\\(z-0.925)(z-0.6135)(z-0.2905)^2\\(z^2-1.902z+0.9055)(z^2-1.309z+0.5305)\\(z^2-1.734z+0.9736)(z^2-1.611z+0.9125)\\(z^2-1.338z+0.8926)(z^2-0.7768z+0.9227)\end{array}}{\begin{array}{l}(z+0.9466)(z^2-1.787z+0.8849)\\(z-0.9837)^3(z^2-0.2614z+0.05821)\\(z-0.6699)(z^2-1.716z+0.9619)\\(z-0.5286)(z^2-1.483z+0.9068)\\(z^2-1.214z+0.8528)(z^2-0.5959z+0.7852)\end{array}} \quad (22)$$

$$Q_{Lowpass}(z)=\frac{0.00041655(z+1)^3}{(z-0.8541)(z^2-1.832z+0.8549)} \quad (23)$$

$$Q_{Bandpass}(z)=\frac{0.00030812(z-1)^3(z+1)^3}{\begin{array}{l}(z-0.9798)(z^2-1.986z+0.9863)\\(z-0.8856)(z^2-1.859z+0.8804)\end{array}} \quad (24)$$

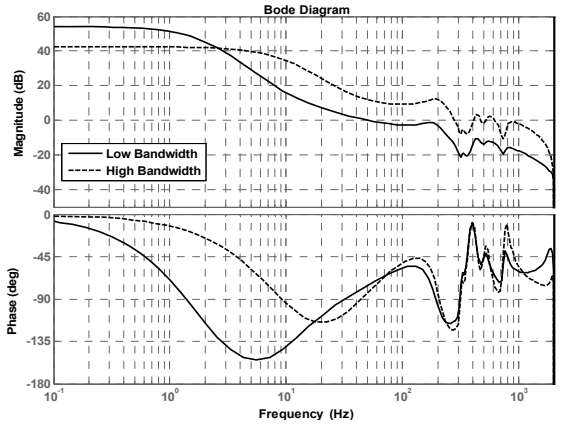

Figure 7. Bode Plot of H_∞ Controller Designs

Two digital, 3rd order, Butterworth Q-filters were designed for ILC. These were a low pass (0-100Hz) and band pass (10-100Hz) Q-filter, (23) and (24), respectively. Table 3 summarizes the four different control scenarios.

Table 3 - Feedback and ILC Controller Combinations

Four Control Scenarios		ILC Q-filter Design	
		Low Pass	Band Pass
H_∞ Feedback Controller Designs	Low Bandwidth	*Reduce Low Frequency disturbance*	*Approach presented here*
	High Bandwidth	*Typical Design*	*Approach presented here*

As with the experimental results of Section 5, the total simulation time was 1.5 seconds. For the simulation tests, $n_j(z)=d(z)=0$, as depicted in Figure 1, and the non-repeating output disturbance was a DC offset defined as $d_j(z)=\Gamma * w_j$ μm, where w_j was a random real-valued constant varying between -1 μm and $1\mu m$. Each set of simulation tests ran for 60 iterations, and the disturbance gain, Γ, varied for each simulation test set. The primary performance measurement was the root mean squared (RMS) value of the error signal. Calculating the RMS was done by (25).

$$e_{RMS}=\frac{\sqrt{\sum_i^N |e_i|^2}}{\sqrt{N}} \quad (25)$$

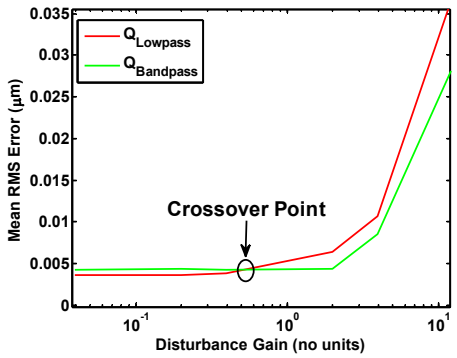

Figure 8. Mean RMS Error vs. Disturbance Gain

The simulated mean RMS error results of the band pass and low pass Q-filter ILC schemes, using the low bandwidth H_∞ controller (21), are plotted against the disturbance gain, Γ, in Figure 8. As Γ is increased, the low frequency content of the nonrepeatable signal increases.

If the low frequency non-repeating signal is relatively small, then the low pass and band pass Q-filter have similar performance, because the exogenous signals have frequency content in only the mid-range frequency (10-30 Hz) region. As the low frequency non-repeating content of the exogenous signals increases (as Γ increases), it enters into the learning update of the low pass Q-filter ILC, which prevents convergence of the ILC control signal. For the band pass Q-filter ILC, the nonrepetitive content does not contribute to the learning control signal, since it is outside the frequency range of learned signals. Therefore, as the content of the low frequency non-repeating signal increases (as Γ increases), Figure 8 indicates that the best design option, for this particular case, is to remove the low frequency content of the exogenous signals from the feedforward learning update by filtering it, i.e. band pass Q-filtering. The feedback control would then be assigned responsibility for mitigating the low frequency disturbance.

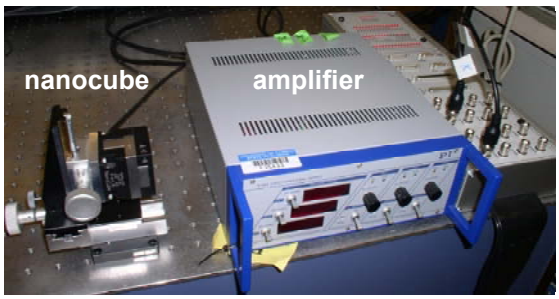

Figure 9. Experimental Setup

V. Experimental Example: Nanopositioner

The controllers of Section 4 were implemented by a DS1104 dSPACE DSP controller board. A layout of the experimental setup can be viewed in Figure 9. For baseline comparison, the feedback controllers in Figure 7 were tested by tracking the sinusoidal reference signal, see Figure 10. As expected, these plots show that the high bandwidth H_∞ controller performs better, i.e. lower tracking error, than the low bandwidth one when operating without ILC.

As previously mentioned, hysteresis is not uncommon in precision motion control systems driven by piezos. As illustrated in Figure 10, the high bandwidth feedback controller would typically be considered a better controller than the low bandwidth one. However, this is not the case when the feedback controllers are combined with ILC. The non-repetitive hysteresis affects the two degree-of-freedom design in a somewhat counterintuitive manner. Figure 11 shows the results of tracking the sinusoidal command, presented in Section 4, when using two of the four control scenarios listed in Table 3. As shown in Figure 11, after a few iterations the RMS tracking error is reduced significantly over feedback alone. The low bandwidth controller scenarios have an initial RMS error that is much larger than that of the high bandwidth controller. However, the low bandwidth feedback controller integrates better with the ILC than the high bandwidth feedback controller in both ILC scenarios, which is observed in the Table 4 statistics. These values were tabulated from the same experimental test results in Figure 11, and only used the iterations after convergence (iterations 3-60) for the mean and standard deviation calculations. Results in Table 4 show quantitative improvements of over 20% error reduction when using $K_{LBW}+Q_{Bandpass}$ as opposed to the typical $K_{HBW}+Q_{Lowpass}$ configuration. As low frequency nonrepetitive exogenous signal content within the system increases this band pass Q-filter approach will provide further benefit as explained in the simulation results of Section 4.

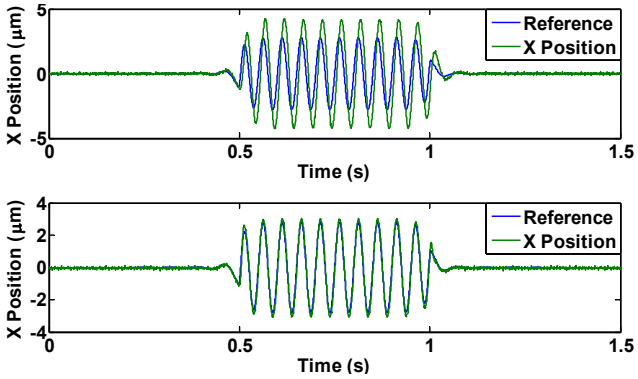

Figure 10. (a) K_{LBW} Feedback Tracking Results (b) K_{HBW} Feedback Tracking Results

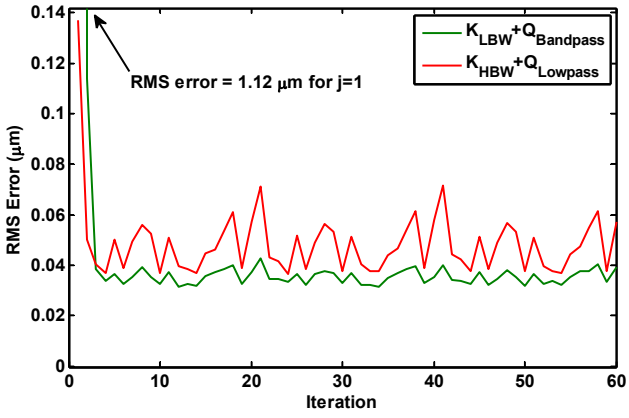

Figure 11. RMS Error from 3µm 20Hz Sinusoid Reference

The results in Figure 11 and Table 4 are explained by re-examining Figures 2, 6, and 7. The hysteresis effect, leading to non-repeating initial conditions, is primarily low frequency, and the reference signal is mid-frequency. Therefore, the successful design should have the feedback controller focus on suppressing disturbances in the low frequency range. The low bandwidth feedback controller has a higher DC gain than its high bandwidth counterpart and is therefore more successful at eliminating the low

frequency effect. The feedback controller then relies on the ILC to provide appropriate reference tracking signals in the mid-range frequency. When low frequency nonrepetitive signal content is large enough, a band pass Q-filter design shows an additional improvement in performance compared to a low pass Q-filter.

Table 4 - Statistics from RMS Error Signals of Experimental Sine Wave Tests (iterations 3-60)

RMS error statistics for all four controller scenarios (iter. 3-60)			ILC Q-filter Design	
			Low Pass	Band Pass
Feedback	Low Bandwidth	Mean	35.9 nm	35.4 nm
		Standard Dev.	3.3 nm	2.8 nm
	High Bandwidth	Mean	46.0 nm	41.1 nm
		Standard Dev.	8.0 nm	3.6 nm

VI. Conclusion

This work presents a design approach for frequency domain allocation of control authority for feedback + feedforward systems; in particular, H_∞ and ILC. Examining frequency content of non-repeating exogenous signals indicates where, within the limitations of the Bode Integral, the feedback sensitivity function should be minimized. In these frequency ranges, ILC contributions can be minimized by shaping the Q-filter to prevent learning. This design approach is in contrast to many ILC applications where the feedback design is often decoupled from the ILC design. Simulation and experimental results were presented demonstrating the validity of the proposed approach. While the data sets (disturbances, references) were limited, further results similar to Sections 4 and 5, with different trajectories and disturbances, can be found in [21].

Acknowledgment

The authors would like to thank Dr. Jennifer Lewis for the use of the PI-611.3S NanoCube for experimental results.

References

[1] D.A. Bristow and A.G. Alleyne, "A High Precision Motion Control System with Application to Microscale Robotic Deposition," *IEEE Control Systems Technologies*, vol. 14, no. 6, pp 1008-1020, 2006.

[2] S. Devasia, E. Eleftheriou, and S.O.R. Moheimani, "A Survey of Control Issues in Nanopositioning," *IEEE Control Systems Technology*, vol. 15, no. 5, pp. 802-823, 2007.

[3] J.C. Doyle, B.A. Francis, and A.R. Tannenbaum, *Feedback Control Theory*. New York: Macmillan, 1992.

[4] S. Skogestad and I. Postlethwaite, *Multivariable Feedback Control, Analysis and Design*. England: Wiley, 2005.

[5] S. Arimoto, S. Kawamura, and F. Miyazaki, "Bettering operation of robots by learning," *Journal of Robotic Systems*, vol. 1, pp. 123-140, 1984.

[6] K.L. Moore, *Iterative Learning Control for Deterministic Systems*. London: Springer-Verlag, 1993.

[7] Z. Bien and J.-X. Xu, *Iterative Learning Control: Analysis, Design, Integration and Applications*. Boston: Kluwer, 1998.

[8] D.A. Bristow, M. Tharayil, and A.G. Alleyne, "A Survey of Iterative Learning Control," *IEEE Control Systems Magazine*, vol. 26, no. 3, pp. 96-114, 2006.

[9] A. Sebastian and S.M. Salapaka, "Design Methodologies for Robust Nano-Positioning," IEEE Control Systems Technology, vol. 13, no. 6, pp. 868-876, 2005.

[10] B. Dijkstra, "Iterative Learning Control with applications to a wafer-stage," Ph.D. thesis, Dutch Institute of Systems and Control, Delft, Netherlands, 2004.

[11] Z.Z. Liu, F.L. Luo, and M.A. Rahman, "Robust and Precision Motion Control System of Linear-Motor Direct Drive for High-Speed X-Y Table Positioning Mechanism," *IEEE Transactions on Industrial Electronics*, vol. 52, no. 5, pp. 1357-1363, 2005.

[12] H.W. Bode, *Network Analysis and Feedback Amplifier Design*. Princeton, NJ: Van Nostrand, 1945.

[13] J. Freudenberg and D. Looze, "Right half plane poles and zeros and design tradeoffs in feedback systems," *IEEE Transactions on Automatic Control*, vol. 30, no. 6, pp. 555-565, 1985.

[14] B.-F. Wu and E.A. Jonckheere, "A Simplified approach to bode's theorem for continuous-time and discrete-time systems." *IEEE Transactions on Automatic Control*, vol. 37, no. 11, pp. 1797-1802, 1992.

[15] H. Kwakernaak, "Robust Control and H_∞-Optimization-Tutorial Paper," *Automatica*, vol. 9, no. 2, pp. 255-273, 1993.

[16] G. Balas, R. Chiang, A. Packard, and M. Safanov, Robust Control Toolbox 3. Natick, MA: The MathWorks, Inc, 2007.

[17] Sogo, T., "Stable Inversion for Nonminimum Phase Sampled-Data Systems and Its Relation With the Continuous-Time Counterpart," *Proceedings of the IEEE Conference on Decision and Control*, pp. 3730-3735, 2002.

[18] D.A. Bristow, "Frequency Domain Analysis and Design of Iterative Learning Control for Systems with Stochastic Disturbances," *submitted to the American Controls Conference*, 2008.

[19] T. Kavli, "Frequency domain synthesis of trajectory learning controllers for robot manipulators," *Journal of Robotic Systems*, vol. 9, no. 5, pp. 663-680, 1992.

[20] M. Goldfarb and N. Celanovic, "Modeling piezoelectric stack actuators for control of micromanipulation," *IEEE Control Systems Magazine*, vol. 13, no. 3, pp. 69-79, 1997.

[21] B.E. Helfrich, "Coordinated Design of H_∞ and Iterative Learning Control for Different Classes of Exogenous Signals," M.S. thesis, Department of Mechanical Science and Engineering, University of Illinois at Urbana-Champaign, Urbana, IL 2008.